Structural Distortions of the $[Fe_4S_4]^{2+}$ Core of $[Fe_4S_4(S\text{-}t\text{-}C_4H_9)_4]^{2-}$ in Different Crystalline Environments and Detection and Instability of Oxidized ($[Fe_4S_4]^{3+}$) Clusters

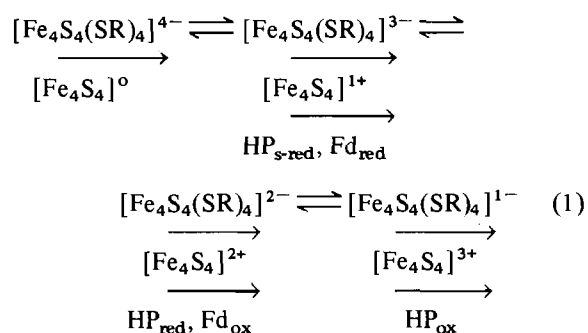P. K. MASCHARAK, K. S. HAGEN, J. T. SPENCE* and R. H. HOLM**

Department of Chemistry, Harvard University, Cambridge, Mass. 02138, U.S.A.

Received February 16, 1983

The structural and redox chemistry of the clusters [Fe₄S₄(SR)₄]²⁻ with R = t-alkyl have been investigated for the purpose of determining the structures of the same cluster in different environments and the stability of the oxidized species [Fe₄S₄(SR)₄]¹⁻. (Me₃NCH₂Ph)₂[Fe₄S₄(S-t-Bu)₄] crystallizes in the monoclinic space group P2₁/c with no imposed symmetry. (Et₄N)₂[Fe₄S₄(S-t-Bu)₄] crystallizes in the tetragonal space group I4̄2m with D₂d symmetry imposed on the cluster. The [Fe₄S₄]²⁺ cluster cores in both compounds exhibit compressed tetragonal structures with different extents of distortion from T_d symmetry. These structures are compared to those of other [Fe₄S₄]²⁺ clusters by means of core shape parameters. Clusters with R = t-alkyl (t-Bu, C(CH₃)₂CH₂OH, C(CH₃)₂CH₂NHPh) in DMF exhibit, in addition to the usual 2–/3– and 3–/4– redox reactions common to all [Fe₄S₄(SR)₄]²⁻ species, discrete one-electron oxidations near −0.1 V vs. s.c.e. Cyclic voltammetry of [Fe₄S₄(S-t-Bu)₄]²⁻ reveals an essentially reversible 1–/2– couple with E₁/₂ = −0.12 V, supporting the authenticity of clusters containing an oxidized ([Fe₄S₄]³⁺) core. This couple cannot be electrochemically resolved from multi-electron oxidation in the case of clusters in DMF with other types of R substituents, a behavior apparently due to cathodic potential shifts by t-alkyl groups. Stability of oxidized clusters is low, and [Fe₄S₄(S-t-Bu)₄]¹⁻ could not be generated in appreciable concentrations at longer times by coulometric or chemical oxidation. The relative stabilities of analogue and protein [Fe₄S₄]³⁺ clusters are discussed. Preparations of four new [Fe₄S₄(SR)₄]²⁻ cluster salts are described including water-soluble (Et₄N)₂[Fe₄S₄(SC(CH₃)₂CH₂OH)₄].

Introduction

In our development of the chemistry of the biologically relevant cubane-type $Fe_4S_4(SR)_4$ clusters, much of which has been summarized [1–4], the electron transfer series (1) has been demonstrated [5,6]. The Fe_4S_4 core oxidation levels of the clusters are indicated together with the oxidation states of ferredoxins (Fd), and its subclass of 'high-potential' (HP) proteins, that contain $Fe_4S_4(S\text{-}Cys)_4$ units iso-electronic wit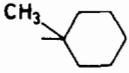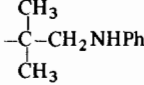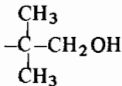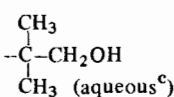h the synthetic clusters. Clusters with $[Fe_4S_4]^{2+}$ and $[Fe_4S_4]^{1+}$ cores are the best defined. The former, readily synthesized by several methods [7–9], exhibit singlet ground states, delocalized electronic structures, and tetragonally compressed cores. This tetragonal distortion, while variable in extent, is a consistent feature of some five clusters whose crystal structures have been determined [7, 10–13]. It is also found in $[Fe_4Se_4(SPh)_4]^{2-}$ [14]. The clusters $[Fe_4S_4(SR)_4]^{3-}$ have been isolated from reduction reactions of the corresponding 2– clusters. These species have paramagnetic ground states, delocalized electronic structures, and $[Fe_4S_4]^{1+}$ core geometries in the crystalline state that, in the three structurally defined cases, are differently distorted from T_d symmetry [15–17]. The isolectronic relationships between $[Fe_4S_4]^{2+,1+}$ and the respec-

$$[Fe_4S_4(SR)_4]^{4-} \rightleftharpoons [Fe_4S_4(SR)_4]^{3-} \rightleftharpoons$$

$$\underset{[Fe_4S_4]^0}{\longrightarrow} \qquad \underset{[Fe_4S_4]^{1+}}{\longrightarrow}$$

$$\underset{HP_{s\text{-}red},\ Fd_{red}}{\longrightarrow}$$

$$[Fe_4S_4(SR)_4]^{2-} \rightleftharpoons [Fe_4S_4(SR)_4]^{1-} \qquad (1)$$

$$\underset{[Fe_4S_4]^{2+}}{\longrightarrow} \qquad \underset{[Fe_4S_4]^{3+}}{\longrightarrow}$$

$$\underset{HP_{red},\ Fd_{ox}}{\longrightarrow} \qquad \underset{HP_{ox}}{\longrightarrow}$$

---

*On leave from the Department of Chemistry, Utah State University, Logan, Utah 84322, U.S.A.
**Author to whom correspondence should be addressed.

TABLE I. Properties of $[Fe_4S_4SR)_4]^{2-}$ Clusters at ~297 K.

R	λ_{max} (ϵ_M), nm DMF	E, V (s.c.e.), DMF[a]			^{1}H NMR Shifts, ppm, CD$_3$CN
		1−/2−	2−/3−	3−/4−	
CH$_3$-cyclohexyl	422 (16,400) 295 (21,000)	b	−1.48	−2.20	−3.77 (CH$_2$), ~−2.7 (CH$_2$), −2.55 (CH$_3$); −1.48, −1.26 (CH$_2$)
−CH−Ph CH$_3$	422 (17,100) 290 (32,000)	b	−1.26	−1.98	−11.34 (CH); −7.40, −6.96 (Ph), ~−3.1 (CH$_3$)
CH$_3$ −C−CH$_2$NHPh CH$_3$	410 (18,600) 305 (32,000)	+0.01	−1.22	−1.92	−7.10(2), −6.67(2), −6.54(1) (Ph); −4.55 (CH$_2$), −4.37 (NH), −2.66 (CH$_3$)
CH$_3$ −C−CH$_2$OH CH$_3$	400 (15,500) 300 (20,500)	−0.07	−1.23	−1.88	−4.31 (CH$_2$), −2.60 (CH$_3$), −2.32 (OH)
CH$_3$ −C−CH$_2$OH CH$_3$ (aqueous[c])	375 (13,900) 300 (17,800)	b	−0.83	d	e
−C(CH$_3$)$_3$	417 (16,700) 303 (21,800)[c]	−0.14	−1.42[f]	−2.16[f]	−2.65[g]

[a]E_p (DPP).   [b]Ill-defined process.   [c]Tris-HCl buffer, pH 8.40, 50 mM thiol added.   [d]Obscured by background reduction.
[e]Not measured.   [f]Ref. 5, dc polarography.   [g]297 K; ref. 31.

tive protein forms have been established by near-coincidences of a variety of spectroscopic and magnetic properties [1–4]. Further, the compressed tetragonal distortion occurs in protein $[Fe_4S_4]^{2+}$ cores [18].

Of the two remaining members of series (1), the terminal reduced species has been detected electrochemically [5, 6]. Attempts to isolate $[Fe_4S_4(SR)_4]^{4-}$ clusters have failed, presumably because of their extreme sensitivity to oxidation ($E_{1/2}(3-/4-) \leqslant -1.7$ V vs. s.c.e.). The $[Fe_4S_4]^0$ core has been isolated only in the form of the carbonyl derivative $Fe_4S_4(CO)_{12}$ [19]. There is no clear evidence that $[Fe_4S_4]^0$ is a physiologically significant oxidation level of Fd proteins. Indication of the existence of the terminal oxidized series member, $[Fe_4S_4(SR)_4]^{1-}$, has rested on the single observation of an oxidative dc polarographic wave with $E_{1/2} = -0.12$ V for $[Fe_4S_4(S-t-Bu)_4]^{2-}$ in DMF solution [5]. The $[Fe_4S_4]^{3+}$ oxidation level has not been demonstrated in conventional Fd proteins, i.e., those which display the reversible Fd_{ox}/Fd_{red} couple at ca. −0.4 V vs. n.h.e. Recent research has shown that 'super-oxidized' forms of such proteins, generated by oxidation of Fd_{ox} forms [20, 21], actually contain 3-Fe clusters [18, 22–25]. Those clusters produced by deliberate chemical oxidation are formed by irrever-

sible oxidative damage of the native clusters of the Fd_{ox} proteins. Existence of the $[Fe_4S_4]^{3+}$ core in proteins has been supported by crystallographic studies of the HP_{red} and HP_{ox} forms from *Chromatium vinosum* [18, 26]. The HP_{ox}/HP_{red} potential for this and similar proteins is ca. +0.3 V vs. n.h.e.

In view of the foregoing results we have examined the oxidation reactions of a number of $[Fe_4S_4(SR)_4]^{2-}$ clusters, primarily by electrochemical means, in order to assess the existence and intrinsic stability of the $[Fe_4S_4]^{3+}$ core in thiolate clusters not subject to the stabilizing/destabilizing influences of protein structure. In the course of this work several new $[Fe_4S_4(SR)_4]^{2-}$ species have been synthesized and the structures of $[Fe_4S_4(S-t-Bu)_4]^{2-}$ in two different crystalline environments have been determined. As indicated by previous results [5] and shown more fully here, this is a satisfactory precursor cluster for examination of oxidation reactions.

Experimental

Preparation of Compounds

All operations were carried out under a pure dinitrogen atmosphere with use of freshly degassed solvents.

Thiols

2-Hydroxymethyl-propane-2-thiol. To a solution of 8.0 g (0.21 mol) of lithium aluminum hydride in 100 ml of THF was added slowly with stirring 40 g (0.19 mol) of α,α'-dithioisobutyraldehyde [27] in 100 ml of THF. After the addition was complete (~1 hr) the reaction mixture was refluxed for 4 hr. The mixture was quenched with H_2SO_4/ice and was extracted with 3 × 100 ml of isopropyl ether. The organic layers were combined, dried ($MgSO_4$), and the solvent was removed *in vacuo*. The pale yellow oily residue was distilled *in vacuo* to afford 30 g (73%) of the thiol as a colorless gel-like material. ^{1}H NMR ($CDCl_3$): δ 3.43 (CH_2), 3.16 (OH), 1.76 (SH), 1.30 (Me).

2-N-anilinomethyl-propane-2-thiol. A solution of 57 g (0.16 mol) of the disulfide ($PhN=CHC(CH_3)_2$-$S)_2$ [27] in 180 ml of THF was added slowly to 11 g (0.19 mol) of lithium aluminum hydride in 150 ml of THF. After the mixture was refluxed for 4 hr it was worked up following the preceding preparation. Distillation of the pale yellow oily residue at 110–115°/0.5 Torr afforded 40 g (69%) of the thiol as a colorless oil. ^{1}H NMR (CCl_4): δ 6.5–7.2 (m, Ph), 3.86 (NH), 2.96 (CH_2), 1.63 (SH), 1.27 (Me).

$(Et_4N)_2[Fe_4S_4(SR)_4]$

All compounds were prepared by standard procedures [7–10]. Spectroscopic and electrochemical properties are collected in Table 1.

$(Et_4N)_2[Fe_4S_4(SCMe_2CH_2OH)_4]$

To a solution of 57 mmol of $Na(SCMe_2CH_2OH)$ (from 1.3 g of sodium and 6.0 g of thiol) in 120 ml of methanol was added 2.3 g (14 mmol) of $FeCl_3$ in 40 ml of methanol. Lithium sulfide (0.65 g, 14 mmol) was added to the deep scarlet reaction mixture, resulting in a rapid color change to red-brown. This mixture was stirred for 16 hr. A solution of 2.5 g (12 mmol) of Et_4NBr in 40 ml of methanol was introduced and the volume of the mixture was reduced to ~50 ml. Upon slow addition of 150 ml of 1:3 v/v THF/ether a black crystalline solid separated. After the mixture was cooled at −20 °C for 6 hr, the solid was collected and treated with 150 ml of warm (~50 °C) propionitrile. The greenish-brown filtrate from this treatment was condensed to ~50 ml and cooled to −20 °C. The solid was collected, washed with 20 ml of 1:6 v/v methanol/ether, and dried *in vacuo*; 1.8 g of product as dark black crystals was obtained. An additional 0.88 g of product (total yield 77%) was recovered by addition of 60 ml of ether to the filtrate. *Anal.* Calcd. for $C_{32}H_{76}$-$Fe_4N_2O_4S_8$: C, 37.21; H, 7.42; Fe, 21.63; N, 2.71;

S, 24.84. Found: C, 36.96, H, 7.44; Fe, 21.42; N, 2.83; S, 24.66.

$(Et_4N)_2[Fe_4S_4(SCMe_2CH_2NHPh)_4]$. To a solution of 1.74 g (1.80 mmol) of $(Et_4N)_2[Fe_4S_4(S$-t-$Bu)_4]$ [28] in 30 ml of DMF was added 1.61 g (8.94 mmol) of $PhNHCH_2CMe_2SH$ in 15 ml of DMF. The reaction mixture was maintained at ~50 °C under partial vacuum for 30 min (to remove liberated t-butylthiol) and then all volatiles were removed from the solution at ~50 °C under full vacuum. The dark oily residue was dissolved in 75 ml of warm acetonitrile (~55 °C) and the solution was filtered. The product (1.84 g, 77%) separated as black crystals upon slow cooling of the filtrate. *Anal.* Calcd. for $C_{56}H_{96}Fe_4N_6S_8$: C, 50.45; H, 7.26; Fe, 16.75; N, 6.30; S, 19.24. Found: C, 50.49; H, 7.15; Fe, 16.82; N, 6.45; S, 19.14.

$(Et_4N)_2[Fe_4S_4(SC_6H_{10}$-$1$-$Me)_4]$. A solution of 1.6 g (10 mmol) of $FeCl_3$ in 40 ml of methanol was slowly added to a solution of 40 mmol of $Na(SC_6$-H_{10}-1-$Me)$ (from 0.92 g of sodium and 5.2 g of 1-methylcyclohexane-1-thiol [29]) in 100 ml of methanol. Sulfur (0.32 g, 10 mmol) was added, causing a color change from scarlet red to greenish-brown. The mixture was stirred for 12 hr, filtered, and 2.1 g (10 mmol) of Et_4NBr in 20 ml of methanol was added; the product crystallized. It was recrystallized from hot acetonitrile/methanol to give 2.1 g (75%) of black crystals. *Anal.* Calcd. for $C_{44}H_{92}Fe_4N_2S_8$: C, 46.78; H, 8.21; Fe, 19.79; N, 2.48; S, 22.72. Found: C, 46.80; H, 8.16; Fe, 19.51; N, 2.52; S, 22.81.

$(Et_4N)_2[Fe_4S_4(SCHMePh)_4]$

The preceding preparation on the same scale was employed, but with racemic 1-phenylethanethiol [30]. The reaction mixture was stirred for 20 hr and the product was precipitated by addition of 2.5 g of Et_4NBr in 40 ml of methanol to the filtrate, the volume of which was first reduced to ~60 ml. This material was extracted with 150 ml of warm (~40 °C) acetonitrile, the solution was filtered, and the filtrate volume was reduced to ~40 ml. Addition of 50 ml of methanol and cooling to −20 °C for 10 hr resulted in the isolation of 2.1 g (72%) of product as black shiny needles. *Anal.* Calcd. for $C_{48}H_{76}Fe_4$-N_2S_8: C, 49.66; H, 6.60; Fe, 19.24; N, 2.41; S, 22.09. Found: C, 49.85; H, 6.46; Fe, 19.30; S, 21.98.

Collection and Reduction of X-ray Data

$(Me_3NCH_2Ph)_2[Fe_4S_4(S$-$t$-$Bu)_4]$ (A) was prepared by a standard method [8]. Black crystals of suitable quality were obtained by recrystallization from acetonitrile. A black well-formed crystal of $(Et_4N)_2$-$[Fe_4S_4(S$-t-$Bu)_4]$ (B) was isolated by slow cooling

TABLE II. Crystallographic Data for $(Me_3NCH_2Ph)_2[Fe_4S_4(S-t-Bu)_4]$ (A) and $(Et_4N)_2[Fe_4S_4(S-t-Bu)_4]$ (B).

Quantity	Compound A	Compound B
Formula (mol. wt.)	$C_{36}H_{68}Fe_4N_2S_8$ (1008.86)	$C_{32}H_{76}Fe_4N_2S_8$ (968.87)
a, Å	16.300(3)	11.830(2)
b, Å	11.432(2)	11.830(2)
c, Å	27.269(4)	19.298(7)
β, deg	92.73(1)	–
Vol, Å^3	5075(1)	2701(1)
Crystal system	monoclinic	tetragonal
Space group	$P2_1/c$	$I\bar{4}2m$
d_{calc}, g/cm^3	1.32	1.19
d_{obs}[a]	1.32	1.19
Z	4	2
Radiation	Mo $K_{\bar{\alpha}}$ (0.71069 Å).	
Abs coeff, μ, cm^{-1}	14.9	13.7
Crystal size, mm	0.12 × 0.34 × 0.40	0.22 × 0.40 × 0.44
Scan speed, deg/min	2.9–29.3	2.9–29.3
Scan range, deg	1.8	2.5
Bkgd/scan time ratio	0.25	0.25
Data collected	$\pm h, +k, +l$	$+h, +k, +l$
2θ range, deg	3.0–42.0	3.0–45.0
Unique data (I > 3σ(I))	3402	552
No. of variables	457	70
GOF[b]	1.37	1.32
R, %	4.7	4.0
R_w, %	4.9	3.9

[a]Measured by neutral buoyancy in CCl_4/n-hexane.   [b]Goodness-of-fit (GOF) is defined as $[\Sigma w(|F_o| - |F_c|)^2/(n_o - n_v)]^{1/2}$, where n_o and n_v denote the number of data and variables refined, respectively.

of an acetonitrile solution. Both compounds were sealed under argon in glass capillaries. Diffraction data were collected at ambient temperature on a Nicolet R3m four-circle automated diffractometer equipped with a Mo X-ray tube and a graphite mono-chromator. Data collection parameters and crystal data for both compounds are summarized in Table II. Orientation matrices and unit cell parameters were obtained from 25 machine-centered reflections (20° $\leqslant 2\theta \leqslant 25°$). Intensities of three check reflections measured every ~120 reflections revealed no decay over the duration of data collection. Data reduction and empirical absorption corrections were performed by the programs XTAPE and XEMP, respectively, of the SHELXTL structure determination program package (Nicolet XRD Corporation, Fremont, California, U.S.A.). For compound A the systematic absences $h0l$ ($l = 2n + 1$) and $0k0$ ($k = 2n + 1$) uniquely define the monoclinic space group $P2_1/c$ (No. 14). For compound B the systematic absences hkl ($h + k + l = 2n + 1$) define a body-centered cell. All axial photographs displayed mirror symmetry,

indicating 4/mmm Laue group. Based on two formula weights per unit cell, molecular symmetry considerations indicated the space group $I\bar{4}m2$ (No. 119) or $I\bar{4}2m$ (No. 121). The Patterson function indicated the latter and subsequent solution and refinement of the structure confirmed this choice.

Solution and Refinement of Structures

For compound A the direct methods program SOLV revealed the location of all Fe and S atoms. Least-squares refinement and difference Fourier maps afforded locations of all other non-hydrogen atoms. Isotropic refinement using blocked cascade least-squares procedure converged at R = 8.3%. Disorder of two t-butyl groups (bonded to S(7) and S(8)) was modeled by allowing each group two sets of methyl carbon atoms with 0.5 occupancy factors. Final refinement included anisotropic descriptions of all non-hydrogen atoms except those of the phenyl rings, which were refined as rigid groups (C–C, 1.395 Å) with isotropic thermal parameters. Fixed hydrogen atoms were included on all non-disordered carbon

atoms with a C–H distance of 0.96 Å and thermal parameters set at 1.2X that of the bonded carbon atom. For compound B a Patterson map and direct methods indicated that the anion was located at a special position $(0, 0, ½)$ with $\bar{4}2m$ (D_{2d}) symmetry and with Fe and S atoms on mirror planes $(x, x, z; \bar{x}\bar{x}z; x\bar{x}z; \bar{x}xz)$. A difference Fourier map following anisotropic refinement of Fe and S atom positions revealed the location of all other non-hydrogen atoms. All such atoms in the asymmetric unit of the anion except for one methyl carbon atom (C(3)) lie on the mirror planes. The large thermal parameter of C(3) indicated disorder, which was not successfully modeled. The cation nitrogen atom lies on a special position having 222 symmetry. A disorder of the methyl carbon atom was modeled in terms of two atoms (C(5a), C(5b)) each with a 0.5 occupancy factor. Hydrogen atoms were not included in the final anisotropic refinement of all atoms. Final R factors and related data for both structures are given in Table II.

Other Physical Measurements

Absorption spectra were measured with a Cary Model 219 spectrophotometer. ^1H NMR spectra were obtained with a Bruker WM-300 spectrometer. Chemical shifts of $[Fe_4S_4(SR)_4]^{2-}$ clusters at fields below that of the Me_4Si internal standard are designated as negative, consistent with a frequent convention for paramagnetic molecules. Cyclic voltammetry (CV), differential pulse polarography (DPP), and coulometry were performed with a three-electrode system using a PAR Model 174A polarographic analyzer, a PAR Model 175 waveform generator, and a PAR Model 173 potentiostat equipped with a digital coulometer. Working electrodes were a Beckman platinum inlay electrode (CV and DPP) and a platinum gauze strip (coulometry). For coulometry the counter electrode compartment was separated from the sample solution by a Vycor disc and was filled with the solvent and electrolyte solution. A saturated calomel electrode (s.c.e.), separated from the reference compartment by a Vycor disc, was used as the reference for all potential measurements. Prior to coulometric measurements the electrolyte solution was preelectrolyzed at potentials used for the sample solutions. The supporting electrolyte was $0.1 \ M$ (n-Bu_4N)ClO_4. DMF (Burdick and Jackson high purity, 0.03% H_2O) was dried for 24 h over activated Linde 4A molecular sieves, degassed, and stored under dinitrogen over 4A sieves. All measurements were performed under anaerobic conditions.

Results and Discussion

The early observation that, of various $[Fe_4S_4$-$(SR)_4]^{2-}$ clusters with R = alkyl and Ph, only the R =

TABLE III. Atom Coordinates of $(Me_3NCH_2Ph)_2$ $[Fe_4S_4$-$(S\text{-}t\text{-}Bu)_4]$ (A) and $(Et_4N)_2$ $[Fe_4S_4(S\text{-}t\text{-}Bu)_4]$ (B).

Atom	x	y	z
Compound A			
Fe(1)	0.7428(1)	0.1761(1)	0.2597(1)
Fe(2)	0.7353(1)	0.3340(1)	0.3352(1)
Fe(3)	0.8849(1)	0.2348(1)	0.3141(1)
Fe(4)	0.7681(1)	0.1024(1)	0.3559(1)
S(1)	0.8083(1)	0.3557(2)	0.2650(1)
S(2)	0.6500(1)	0.1749(2)	0.3217(1)
S(3)	0.8408(1)	0.0514(2)	0.2880(1)
S(4)	0.8309(1)	0.2664(2)	0.3899(1)
S(5)	0.6665(1)	0.1358(2)	0.1900(1)
S(6)	0.6707(2)	0.5052(2)	0.3480(1)
S(7)	1.0220(1)	0.2646(2)	0.3157(1)
S(8)	0.7701(2)	−0.0612(2)	0.4023(1)
C(51)[a]	0.7335(5)	0.1216(8)	0.1387(3)
C(52)	0.8000(7)	0.2149(12)	0.1391(5)
C(53)	0.7759(11)	0.0098(13)	0.1431(6)
C(54)	0.6823(8)	0.1307(19)	0.0929(4)
C(61)	0.6303(6)	0.5094(10)	0.4102(4)
C(62)	0.7029(8)	0.5301(13)	0.4470(4)
C(63)	0.5739(8)	0.6140(13)	0.4134(5)
C(64)	0.5890(12)	0.3929(15)	0.4224(6)
C(71)	1.0772(5)	0.1621(9)	0.3601(4)
C(72A)[d]	1.1625(19)	0.2033(27)	0.3714(11)
C(72B)	1.1692(17)	0.1619(34)	0.3444(12)
C(73A)	1.0456(18)	0.0402(20)	0.3626(11)
C(73B)	1.0868(16)	0.0412(17)	0.3288(8)
C(74A)	1.0299(18)	0.1173(33)	0.4047(14)
C(74B)	1.0668(21)	0.2171(33)	0.4098(8)
C(81)	0.7247(7)	−0.0306(10)	0.4623(4)
C(82A)	0.7347(27)	0.0866(27)	0.4812(15)
C(82B)	0.7987(15)	0.0356(19)	0.4917(7)
C(83A)	0.7212(17)	−0.1225(20)	0.4981(11)
C(83B)	0.7361(15)	−0.1597(16)	0.4878(7)
C(84A)	0.6250(25)	−0.0345(37)	0.4486(18)
C(84B)	0.6510(27)	0.0408(34)	0.4591(1)
N(1)	0.0789(4)	0.1795(6)	0.1716(3)
C(10)[b]	0.0277(5)	0.0865(8)	0.1938(4)
C(11)	0.0332(5)	0.2925(7)	0.1703(4)
C(12)	0.1556(5)	0.1969(10)	0.2048(4)
C(13)	0.1052(5)	0.1459(8)	0.1214(3)
C(15)	−0.0068(4)	0.0336(5)	0.0760(2)
C(16)	−0.0715(4)	0.0285(5)	0.0407(2)
C(17)	−0.0925(4)	0.1273(5)	0.0128(2)
C(18)	−0.0487(4)	0.2312(5)	0.0202(2)
C(19)	0.0160(4)	0.2363(5)	0.0555(2)
C(14)	0.0369(4)	0.1375(5)	0.0834(2)
N(2)	0.4237(4)	0.3056(6)	0.2450(3)
C(20)	0.4705(5)	0.2046(8)	0.2268(4)
C(21)	0.4805(6)	0.3823(8)	0.2754(4)
C(22)	0.3875(8)	0.3741(11)	0.2037(5)
C(23)	0.3524(5)	0.2649(9)	0.2737(4)
C(25)	0.3599(4)	0.0579(7)	0.3025(2)
C(26)	0.3784(4)	−0.0263(7)	0.3384(2)
C(27)	0.4099(4)	0.0078(7)	0.3846(2)
C(28)	0.4229(4)	0.1260(7)	0.3951(2)

TABLE III. *(continued)*

Atom	x	y	z
C(29)	0.4044(4)	0.2102(7)	0.3592(2)
C(24)	0.3729(4)	0.1761(7)	0.3129(2)
Compound B			
Fe	0.0826(1)	0.0826(1)	0.4499(1)
S(1)	0.1080(1)	0.1080(1)	0.5657(1)
S(2)	0.2013(2)	0.2013(2)	0.3946(2)
C(1)[c]	0.1852(9)	0.1852(9)	0.2987(7)
C(2)	0.2688(13)	0.2688(13)	0.2662(9)
C(3)	0.0688(13)	0.2194(26)	0.2822(7)
N	0.5000	0	0
C(4)	0.4299(23)	0.0826(13)	0.0409(11)
C(5a)[d]	0.3117(45)	0.0435(37)	0.0584(22)
C(5b)	0.4090(36)	0.0206(29)	0.1138(18)

Numbering schemes: [a]S(n)–C(n1)–C$_3$[n(2–4)], n = 5–8 (anion). [b]C$_3$[n(0–2)] –N(n)–C(n3)–Ph[n(4–9)], n = 1, 2 (cation). [c]S(2)–C(1)$\underset{\text{C(3)}}{\overset{\text{C(2)}}{\diagdown}}$. [d]A, B and a, b refer to positions of disordered carbon atoms.

$(Me_3NCH_2Ph)_2[Fe_4S_4(S\text{-}t\text{-}Bu)_4]$ $(Et_4N)_2[Fe_4S_4(S\text{-}t\text{-}Bu)_4]$

Fig. 1. Structures of the Fe_4S_8 portion of $[Fe_4S_4(S\text{-}t\text{-}Bu)_4]^{2-}$ showing atom labelling schemes, 50% probability ellipsoids, and selected interatomic distances (Å). The $\bar{4}$ axis is idealized in the $(Me_3NCH_2Ph)^+$ salt structure and is imposed in the Et_4N^+ salt structure.

Fig. 2. Stereoview of $[Fe_4S_4(S\text{-}t\text{-}Bu)_4]^{2-}$ illustrating the orientation of t-Bu groups in the $(Me_3NCH_2Ph)^+$ salt (top) and the imposed D_{2d} symmetry of the entire cluster in the Et_4N^+ salt (bottom). The Fe_4S_8 portions have the same orientation as in Fig. 1. Because of apparent disorder of certain atoms, carbon atoms are shown as spheres of arbitrary but constant size whereas Fe and S atoms are depicted in terms of 50% probability ellipsoids.

t-Bu species exhibited a well-defined oxidation in electrochemical experiments [5], has prompted further investigation of clusters with t-alkyl substituents. Properties of three new clusters are set out in Table I. Absorption and ^{1}H NMR spectral properties are consistent with those of other $[Fe_4S_4(SR)_4]^{2-}$ clusters [5, 6, 10, 31, 32] and, together with analytical results, confirm the cluster formulation. Several additional features of the new compounds are noted. $(Et_4N)_2[Fe_4S_4(SCMe_2CH_2OH)_4]$ is freely soluble in polar aprotic solvents, lower alcohols, and water. This compound augments previous examples of cluster salts, containing $[Fe_4S_4(SCH_2CH_2OH)_4]^{2-}$ [13, 32], $[Fe_4S_4(S\text{-}p\text{-}C_6H_4\text{-}OH)_4]^{2-}$ [33] (sparingly soluble), $[Fe_4S_4(S(CH_2)_{2,3}\text{-}CO_2)_4]^{6-}$ [11, 34, 35], and a Fe_4S_4/cysteinylpeptide species [36], with the useful property of aqueous solubility. $(Et_4N)_2[Fe_4S_4(SCHMePh)_4]$ was prepared from the racemic thiol and presumably was obtained as a mixture of diastereomeric anions. However, these were not resolved in the NMR spectrum. The cluster $[Fe_4S_4(S\text{-}t\text{-}Bu)_4]^{2-}$, one of the earliest prepared [7], was isolated here as its $(Me_3NCH_2Ph)^+$ and Et_4N^+ salts in order to examine $[Fe_4S_4]^{2+}$ core structures of the same cluster in two different crystalline environments. This matter has not been previously investigated for any $[Fe_4S_4]^{1+,2+}$ species.

Structures of $[Fe_4S_4(S\text{-}t\text{-}Bu)_4]^{2-}$

The $(Me_3NCH_2Ph)^+$ salt (A) and the Et_4N^+ salt (B) crystallize in monoclinic space group $P2_1/c$ and tetragonal space group $I\bar{4}2m$, respectively. Atomic
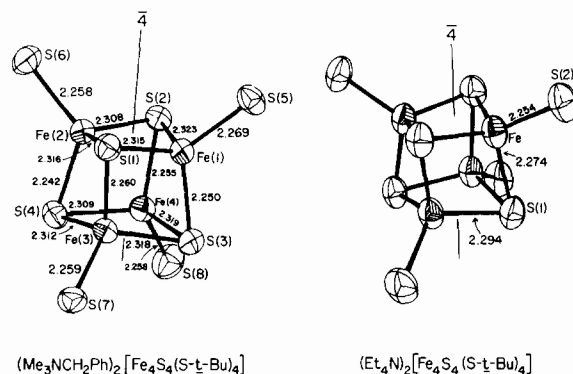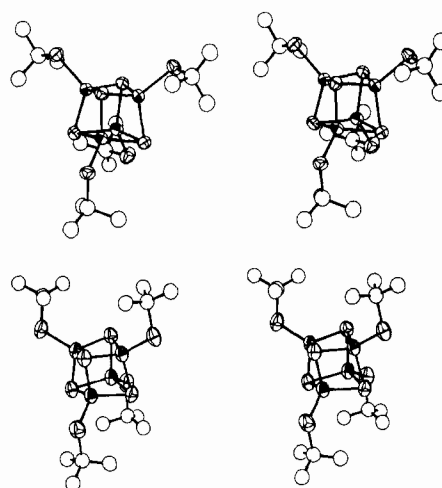
coordinates are compiled in Table III, selected interatomic distances and angles of the clusters are presented in Table IV, and thermal parameters are collected in Table V. Metric parameters of the cations are unexceptional and are not tabulated. Structures of the Fe_4S_8 portions of the cluster are presented in Fig. 1 and stereoviews of the entire cluster are provided in Fig. 2. The crystal structures of both compounds consist of well-separated cations and anions. Both structures evidence problems of disorder. In compound A the substituents S(7,8)-t-Bu are distributed in two sets of methyl carbon atom positions. In compound B one methyl carbon atom

TABLE IV. Selected Interatomic Distances (Å) and Angles (deg) of $[Fe_4S_4^*(S\text{-}t\text{-}Bu)_4]^{2-}$ in its $(Me_3NCH_2Ph)^+$ (A) and Et_4N^+ (B) Salts.

Fe–S*	A	B[b]	Fe–S	A	B
Fe(1)–S(3)	2.250(2)		Fe(1)–S(5)	2.269(3)	
Fe(2)–S(4)	2.242(3)		Fe(2)–S(6)	2.258(3)	
Fe(3)–S(1)	2.260(3)		Fe(3)–S(7)	2.259(2)	
Fe(4)–S(2)	2.255(2)	2.274(3)	Fe(4)–S(8)	2.258(3)	2.254(3)
mean	2.252(8)[a]		mean	2.261(5)	
Fe(1)–S(1)	2.315(2)				
Fe(1)–S(2)	2.323(3)		Fe–Fe–Fe	A	B
Fe(2)–S(1)	2.316(3)		Fe(3)–Fe(1)–Fe(4)	58.9(1)	
Fe(2)–S(2)	2.308(2)		Fe(3)–Fe(2)–Fe(4)	59.0(1)	
Fe(3)–S(3)	2.318(3)		Fe(1)–Fe(3)–Fe(2)	59.3(1)	
Fe(3)–S(4)	2.312(3)		Fe(1)–Fe(4)–Fe(2)	59.6(1)	60.4
Fe(4)–S(3)	2.319(3)		mean	59.2(3)	
Fe(4)–S(4)	2.309(3)	2.294(2)	Fe(2)–Fe(1)–Fe(4)	60.0(1)	
mean	2.315(5)		Fe(2)–Fe(1)–Fe(3)	60.4(1)	
			Fe(1)–Fe(2)–Fe(3)	60.3(1)	
Fe···Fe	A	B	Fe(1)–Fe(2)–Fe(4)	60.4(1)	
Fe(1)–Fe(2)	2.745(2)		Fe(4)–Fe(3)–Fe(1)	60.4(1)	
Fe(3)–Fe(4)	2.723(2)	2.749(2)	Fe(4)–Fe(3)–Fe(2)	60.1(1)	
mean	2.734		Fe(3)–Fe(4)–Fe(1)	60.7(1)	
Fe(1)–Fe(4)	2.766(2)		Fe(3)–Fe(4)–Fe(2)	60.9(1)	59.8
Fe(1)–Fe(3)	2.773(2)		mean	60.4(3)	
Fe(2)–Fe(4)	2.753(2)		mean (of 12)	60.0	60.0
Fe(2)–Fe(3)	2.755(2)	2.764(3)			
mean	2.767(10)				
mean (of 6)	2.756(20)	2.759			

S*–Fe–S*	A	B	S–Fe–S*	A	B
S(1)–Fe(1)–S(2)	105.9(1)		S(5)–Fe(1)–S(3)	120.7(1)	
S(1)–Fe(2)–S(2)	106.4(1)		S(6)–Fe(2)–S(4)	120.7(1)	
S(3)–Fe(3)–S(4)	106.9(1)		S(7)–Fe(3)–S(1)	115.9(1)	
S(3)–Fe(4)–S(4)	107.0(1)	103.9(1)	S(8)–Fe(4)–S(2)	121.6(1)	107.5(1)
mean	106.5(6)		mean	119.7	
S(1)–Fe(1)–S(3)	102.9(1)		S(5)–Fe(1)–S(1)	117.7(1)	
S(2)–Fe(1)–S(3)	102.9(1)		S(5)–Fe(1)–S(2)	105.0(1)	
S(1)–Fe(2)–S(4)	102.6(1)		S(6)–Fe(2)–S(1)	107.3(1)	
S(2)–Fe(2)–S(4)	103.2(1)		S(6)–Fe(2)–S(2)	115.2(1)	
S(1)–Fe(3)–S(3)	102.5(1)		S(7)–Fe(3)–S(3)	115.7(1)	
S(1)–Fe(3)–S(4)	102.2(1)		S(7)–Fe(3)–S(4)	112.3(1)	
S(2)–Fe(4)–S(3)	102.8(1)		S(8)–Fe(4)–S(3)	104.1(1)	
S(2)–Fe(4)–S(4)	102.7(1)	104.0(1)	S(8)–Fe(4)–S(4)	117.0(1)	117.9(1)
mean	102.7(3)		mean	111.8	
mean (of 12)	104.0	104.0	mean (of 12)	115.1	114.4

Fe–S*–Fe	A	B	S–C	A	B
Fe(1)–S(1)–Fe(2)	72.7(1)		S(5)–C(51)	1.822(10)	
Fe(1)–S(2)–Fe(2)	72.7(1)		S(6)–C(61)	1.848(10)	
Fe(3)–S(3)–Fe(4)	71.9(1)		S(7)–C(71)	1.884(10)	
Fe(3)–S(4)–Fe(4)	72.2(1)	74.1(1)	S(8)–C(81)	1.862(11)	1.870(13)
mean	72.4(4)		mean	1.85(3)	
Fe(1)–S(1)–Fe(3)	74.6(1)				
Fe(2)–S(1)–Fe(3)	74.7(1)				
Fe(1)–S(2)–Fe(4)	74.3(1)		C–C[c]	A	B
Fe(2)–S(2)–Fe(4)	74.2(1)		range	1.46(2)–1.54(2)	1.53(3)
Fe(1)–S(3)–Fe(3)	74.7(1)		mean	1.51(3)	
Fe(1)–S(3)–Fe(4)	74.5(1)				
Fe(2)–S(4)–Fe(3)	75.1(1)				

TABLE IV. *(continued)*

Fe–S*–Fe	A	B	S–C	A	B
Fe(2)–S(4)–Fe(4)	74.4(1)	74.0			
mean	74.6(3)				
mean (of 12)	73.9	74.0			

[a]The standard deviation of the mean is estimated from $\sigma \approx s = [(\Sigma x_i^2 - n\bar{x}^2)/(n - 1)]^{1/2}$. No value is given when the variations exceed those expected from a sample taken from the same population. [b]Atom numbering scheme does not apply. [c]Disordered atoms excluded.

TABLE V. Anisotropic Temperature Factors[a] ($\text{Å}^2 \times 10^3$) for $Me_3NCH_2Ph)_2[Fe_4S_4(S\text{-}t\text{-}Bu)_4]$ (A) and $(Et_4N)_2[Fe_4S_4(S\text{-}t\text{-}Bu)_4]$ (B).

Atom	U_{11}	U_{22}	U_{33}	U_{23}	U_{13}	U_{12}
Compound A						
Fe(1)	40(1)	44(1)	45(1)	−4(1)	−2(1)	−1(1)
Fe(2)	42(1)	43(1)	51(1)	−5(1)	−2(1)	4(1)
Fe(3)	36(1)	46(1)	51(1)	−3(1)	−2(1)	0(1)
Fe(4)	44(1)	47(1)	47(1)	2(1)	−3(1)	2(1)
S(1)	49(1)	42(1)	53(2)	5(1)	−1(1)	−1(1)
S(2)	36(1)	50(1)	55(2)	−3(1)	−0(1)	−0(1)
S(3)	45(1)	44(1)	57(2)	−3(1)	1(1)	5(1)
S(4)	48(1)	59(1)	47(1)	−8(1)	−6(1)	1(1)
S(5)	40(1)	80(2)	47(2)	−9(1)	3(1)	−5(1)
S(6)	63(2)	50(2)	64(2)	−3(1)	6(1)	13(1)
S(7)	39(1)	52(1)	73(2)	2(1)	1(1)	0(1)
S(8)	93(2)	55(2)	61(2)	9(1)	5(1)	8(1)
C(51)	62(6)	62(6)	52(6)	−11(5)	10(5)	−3(5)
C(52)	91(9)	191(15)	103(10)	−44(11)	55(8)	−60(10)
C(53)	238(19)	114(12)	194(17)	22(12)	159(16)	61(13)
C(54)	101(10)	445(32)	44(9)	−26(15)	1(7)	−23(16)
C(61)	69(7)	88(8)	57(7)	−28(6)	7(5)	2(6)
C(62)	123(11)	152(13)	69(9)	−25(9)	−3(7)	38(10)
C(63)	120(11)	185(16)	89(10)	−44(10)	5(8)	70(10)
C(64)	285(23)	152(15)	144(15)	−44(12)	137(15)	−110(15)
C(71)	45(5)	78(7)	68(7)	6(6)	−7(5)	7(5)
C(72A)	66(17)	83(20)	91(26)	−4(17)	−35(18)	−16(14)
C(72B)	32(12)	170(35)	95(27)	−12(22)	−12(16)	20(18)
C(73A)	166(26)	48(14)	112(24)	21(15)	−66(21)	−29(15)
C(73B)	167(23)	34(11)	81(17)	9(12)	−43(16)	29(13)
C(74A)	92(20)	144(30)	134(32)	85(27)	42(20)	30(21)
C(74B)	176(30)	196(32)	24(14)	26(19)	−2(16)	138(27)
C(81)	132(10)	70(8)	53(8)	3(6)	19(7)	−18(7)
C(82A)	379(52)	107(24)	239(40)	−121(26)	230(39)	−110(29)
C(82B)	159(22)	86(16)	34(13)	−18(12)	−9(13)	−53(16)
C(83A)	166(25)	57(16)	137(25)	−9(16)	43(20)	38(16)
C(83B)	199(24)	38(11)	21(11)	13(10)	39(13)	9(13)
C(84B)	122(35)	141(36)	134(34)	31(31)	63(27)	44(26)
C(84A)	82(22)	179(43)	107(28)	24(32)	36(19)	3(26)
N(1)	34(4)	42(4)	66(5)	−0(4)	−3(3)	4(3)
C(10)	60(6)	53(6)	62(7)	1(5)	−8(5)	0(5)
C(11)	62(6)	46(6)	77(8)	−4(6)	4(5)	9(5)
C(12)	47(6)	82(8)	93(9)	−20(7)	−22(6)	−4(5)
C(13)	49(5)	69(7)	56(7)	1(5)	12(5)	8(5)
N(2)	50(4)	48(5)	74(6)	−0(4)	−5(4)	15(4)
C(20)	53(6)	54(6)	97(9)	−13(6)	4(6)	10(5)

TABLE V. (continued)

Atom	U_{11}	U_{22}	U_{33}	U_{23}	U_{13}	U_{12}
C(21)	79(7)	56(7)	87(9)	−15(6)	13(6)	−3(6)
C(22)	114(10)	108(10)	115(12)	33(9)	−3(9)	49(8)
C(23)	35(5)	90(8)	117(10)	−9(8)	16(6)	2(6)
Compound B						
Fe	51(1)	51(1)	78(1)	5(1)	5(1)	−1(1)
S(1)	56(1)	56(1)	84(2)	−5(1)	−5(1)	−6(1)
S(2)	70(1)	70(1)	106(2)	13(1)	13(1)	−13(1)
C(1)	119(5)	119(5)	82(5)	23(4)	23(4)	−11(6)
C(2)	211(6)	211(6)	120(6)	43(5)	43(5)	−76(7)
C(3)	137(6)	698(7)	87(5)	86(7)	−25(5)	−26(7)
N	382(7)	43(5)	96(6)	0	0	0
C(4)	369(7)	100(6)	289(7)	−49(6)	16(7)	18(7)
C(5a)	417(7)	219(7)	218(7)	−24(7)	−45(7)	123(7)
C(5b)	447(7)	163(7)	224(7)	−74(7)	212(7)	−111(7)

[a]The anisotropic temperature factor is of the form $\exp[-2\pi^2(U_{11}h^2a^{*2} + U_{22}k^2b^{*2} + U_{33}l^2c^{*2} + 2U_{12}hka^*b^* + 2U_{13}hla^*c^* + 2U_{23}klb^*c^*)]$.

of the equivalent t-Bu groups apparently is disordered as is a similar atom of the cation. All N, Fe, and S atoms are well-behaved. Both structures refined to acceptable R-values (Table II).

The principal structural features of $[Fe_4S_4(S\text{-}t\text{-}Bu)_4]^{2-}$ in its two salts are generally similar to each other and to those of the five other clusters with $[Fe_4S_4]^{2+}$ cores presented for comparison purposes in Table VI. For this reason and because structures of this type have been analyzed in detail elsewhere [4, 7], these features are described rather briefly. (*i*) The cores consist of nearly concentric, imperfect Fe_4 and S_4 tetrahedra. The volume of the latter is ~2.3 times larger than that of the former. (*ii*) Core Fe_2S_2 faces are decidedly non-planar rhombs; the six diagonal planes through the core are nearly perfect. (*iii*) No symmetry is imposed on the cluster in compound A but its core approaches D_{2d} symmetry. Under this idealized symmetry the core distances Fe–S (4 + 8), Fe–Fe (2 + 4), and S–S (2 + 4) and angles S–Fe–S (4 + 8), Fe–S–Fe (4 + 8), Fe–Fe–Fe (4 + 8), and RS–Fe–S (4 + 8) divide into the indicated sets, which are grouped accordingly in Table IV. (*iv*) The sense of the tetragonal distortion in compound A is such that four 'short' Fe–S bonds of mean length 2.252(8) Å are approximately parallel to the idealized $\bar{4}$ axis, and the eight 'long' Fe–S bonds, which average to 2.315(5) Å, are roughly perpendicular to this axis. (*v*) In compound B D_{2d} symmetry is crystallographically imposed on the cluster, as may be seen in the stereoview of Fig. 2. With reference to the true $\bar{4}$ axis of this cluster (Fig. 1) the parallel and perpendicular Fe–S bonds are short (2.274(3) Å) and long (2.294(2) Å, respec-

tively. (*vi*) In both compounds the (mean) Fe–Fe distances occur as two short and four somewhat longer separations, resulting in Fe_4 tetrahedra that are slightly distorted along the $\bar{4}$ axis. (*vii*) Departure of the Fe_4S_8 cluster portion in compound A from D_{2d} symmetry is emphasized by the large variations within each set of 4 + 8 RS–Fe–S angles. This is a frequent aspect of the structure of other clusters in Table VI. The sensitivity of angles of this type to crystalline environment is evident from the fact that the (mean) angles in the two sets are in the reverse order for compounds A and B.

Structural Comparisons of Clusters

Contained in Table VI are data for all $[Fe_4S_4]^{2+}$ clusters whose structures have been published. Another such cluster, $[Fe_4S_4(OPh)_4]^{2-}$ [37], has quite similar structural properties [38]. For the purpose of systematic structural comparisons amongst M_4X_4 cubane-type clusters with tetragonal distortions the shape parameters r and β have been introduced [4]. These parameters are defined with respect to a coordinate origin given by the mean of coordinates (from X-ray analysis) of the eight atoms and a $\bar{4}$ axis which passes through the origin and the centers of M–M and X–X segments on opposite faces. The four independent values of each parameter are averaged. The distance r is that from the origin to atom M or X and β is the polar angle between the $\bar{4}$ axis and the vector r. Relationships between the distance d(M–X), r_M, r_X, β_M, β_X, and $V(M_4, X_4)$ have been derived and are given elsewhere [4]. For a perfect tetrahedron $\beta_{tetr} = 54.74°$. Shape parameters are entered in Table VI together with volumes

TABLE VI. Structural Comparisons of $[Fe_4S_4^*(SR)_4]$ Clusters with $[Fe_4S_4^*]^{2+}$ Cores.

R	Distance, Å					Angle, deg		Vol., Å³			Ref.[b]
	Fe–Fe	Fe–S*	Fe–S	r_{Fe}	r_{S*}	β_{Fe}	β_{S*}	Fe_4[a]	S_4^*[a]	$Fe_4S_4^*$	
CH_2Ph	2[c] at 2.776 / 4 at 2.732(5)	4 at 2.239(7)[d] / 8 at 2.310(8)	2.251(5)	1.682(4)	2.208(5)	55.6(2)	55.6(2)	2.44	5.52	9.61	7
Ph	2 at 2.730 / 4 at 2.739(8)	4 at 2.267(9) / 8 at 2.296(12)	2.263(7)	1.675(2)	2.211(7)	54.6(3)	55.6(1)	2.41	5.54	9.55	10
$CH_2CH_2CO_2$	2 at 2.778 / 4 at 2.743(8)	4 at 2.261(7) / 8 at 2.300(8)	2.250(3)	1.687(2)	2.206(5)	55.4(2)	55.0(1)	2.46	5.50	9.66	11
CH_2CH_2OH	6[f] at 2.729(18)	4 at 2.239(7) / 8 at 2.307(17)	2.256(18)	1.671(14)	2.212(22)	f	56.5(4)	2.39	5.53	9.50	13
t-Bu (A)[g]	2 at 2.734 / 4 at 2.767(10)	4 at 2.252(8) / 8 at 2.315(5)	2.261(3)	1.688(6)	2.214(5)	54.1(3)	56.9(2)	2.45	5.55	9.68	e
t-Bu (B)[h]	2 at 2.749(2) / 4 at 2.764(3)	4 at 2.274(3) / 8 at 2.294(2)	2.254(3)	1.687(3)	2.207(3)	55.0(1)	54.9(1)	2.47	5.53	9.69	e
Cl[i]	2 at 2.755 / 4 at 2.771(7)	4 at 2.260(9) / 8 at 2.295(7)	–	1.694(5)	2.197(5)	54.4(1)	55.9(2)	2.49	5.43	9.70	12

[a] $V(Q_4) = 4/3 \sqrt{3}\, r_Q^3 \cos\beta_Q \sin^2\beta_Q$ (Q = Fe or S*). [b] Source of crystallographic data; shape parameters and their standard deviations calculated by the method of ref. 4. [c] Number of distances averaged under idealized D_{2d} symmetry. [d] Standard deviation of the mean calculated as in Table IV; original references may use a different estimate. [e] This work. [f] Irregular Fe_4 unit. [g] $(Me_3NCH_2Ph)^+$ salt. [h] Et_4N^+ salt. [i] $[Fe_4S_4Cl_4]^{2-}$.

and mean values of certain bond distances. A full analysis of M_4X_4 stereochemistry will be presented [39]. When compared to molecules with larger tetragonal distortions, such as $(C_5H_5)_4Fe_4S_4$ [40] ($\beta_{Fe} = 43.1°$, 43.5°, $\beta_S = 63.8°$, 63.6° in two crystalline forms) and $[(C_5H_5)_4Fe_4S_4]^{2+}$ [41] ($\beta_{Fe} = 63.1°$, $\beta_S = 47.0°$), the close structural similarity of $[Fe_4S_4]^{2+}$ clusters is even more evident.

The shape parameters reflect small differences in the S_4 and Fe_4 core portions of the different clusters, some of which persist at a $\geqslant 3\sigma$ significance level. In all cases the S_4 units exhibit two long and four short S···S separations, $\beta_S > \beta_{tetr}$ signifying flattened tetrahedral structures, and $V(S_4)$ values which vary by $<1\%$. The Fe_4 tetrahedra are less regular in shape, with examples of two short and four long Fe–Fe bonds and the reverse, and β_{Fe} values indicative of flattened and elongated tetrahedra. Values of $V(Fe_4)$ vary by $\lesssim 4\%$. The most regular Fe_4 tetrahedron is found in $[Fe_4S_4(SPh)_4]^{2-}$ and the least regular in $[Fe_4S_4(SCH_2CH_2OH)_4]^{2-}$. In the same cluster, $[Fe_4S_4(S\text{-}t\text{-}Bu)_4]^{2-}$, the most flattened S_4 and most elongated Fe_4 tetrahedra occur in compound A and, by the β criterion, are essentially equally regular in compound B although this is obviously not a necessity of imposed symmetry. The small differences in Fe_4 structures in this cluster are further indicated by the reversal in Fe–Fe–Fe angles in the two compounds (Table IV).

The preceding results demonstrate that $[Fe_4S_4]^{2+}$ cores are subject to small structural differences, which extend to the case of the same cluster in two different crystalline environments. These differences notwithstanding, the principal structural feature is the tetragonal compression of the cores which, although not uniform in extent, exists in every $[Fe_4S_4]^{2+}$ structure to date. As noted above, this distortion appears in isoelectronic protein clusters [18]. The latest example is *Azotobacter vinelandii* Fd 1, in which the average values of the short and long bonds of the Fe_4S_4 cluster are 2.24 Å and 2.33 Å, respectively [25]. Recent theoretical calculations of the electronic structures of $[Fe_4S_4(SR)_4]^{2-}$ (R = H, Me) by Aizman and Case [42] afford a closed shell ground state in T_d symmetry, thereby disallowing the possibility of distortion to a lower symmetry by the first-order Jahn–Teller effect. This possibility had been suggested from the results of early $X\alpha$ calculations in which the $[Fe_4S_4]^{2+}$ core for simplicity was treated as a cube [43]. Whatever the source of the distortion, the results presented here further support the proposition that a compressed tetragonal geometry, while slightly variable in the extent of compression as dependent on extrinsic environmental factors, is the intrinsically stable structure of $[Fe_4S_4]^{2+}$ cores in clusters having four identical unidentate ligands. In related work we have found that five-coordination at a Fe site can cause sub-
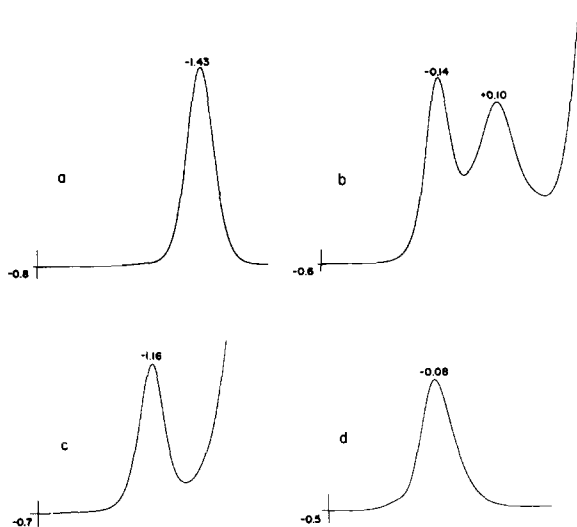
$[Fe_4S_4]^{2+}$ *Clusters* 167

Fig.3. Differential pulse polarograms at a Pt electrode with 5 mV/s scan rate and 25 mV peak-to-peak modulation showing the first reduction (a) and oxidation (b) of [Fe₄S₄-(S-t-Bu)₄]²⁻ in DMF, and the first reduction (c) and oxidation (d) of [Fe₄S₄(SCMe₂CH₂OH)₄]²⁻ in 1:1 v/v DMF/methanol. Peak potentials vs. s.c.e. are given.

Fig. 4. Cyclic voltammograms at a Pt electrode in DMF with a scan rate of 100 mV/s: (a) [Fe₄S₄(SCMe₂CH₂NHPh)₄]²⁻ at −0.8 to −2.2 V; (b) [Fe₄S₄(S-t-Bu)₄]²⁻, initial potential −0.30 V, initial scan direction cathodic (———) and anodic (- - - - -). Peak potentials vs. s.c.e. are given. Note that potential scales for (a) and (b) are in opposite directions.

stantial departure of the core structure from a tetragonal arrangement; these results will be reported separately [44]. Elsewhere we have interpreted properties of [Fe₄S₄(SR)₄]³⁻ clusters in terms of an elongated tetragonal structure as the intrinsically stable form of the [Fe₄S₄]¹⁺ core [15, 17, 45].

Redox Reactions of [Fe₄S₄(SR)₄]²⁻

Reduction

The electrochemical behavior of selected clusters of this type is shown in the form of the differential pulse polarograms of Fig. 3 and the cyclic voltammograms of Fig. 4. All [Fe₄S₄(SR)₄]²⁻ clusters exhibit in aprotic media a chemically reversible 2−/3− couple and a 3−/4− step that most closely approaches reversibility when R = Ph [5, 6, 46]. The situation is illustrated with [Fe₄S₄(SCMe₂-CH₂NHPh)₄]²⁻ in Fig. 4a, where $E_{1/2}$ (2−/3−) = −1.22 V and $E_{1/2}$ (3−/4−) = −1.92 V are observed. A potential separation of ∼0.70 V in DMF, also found here for three other cases (Table I), is a characteristic feature of these clusters [5]. The 2−/3− potential is notably sensitive to aprotic vs. protic solvent and to the nature of the substituent R. Protic solvents cause shifts to less negative potentials, as previously found [32–35]. The potential of [Fe₄S₄(SCMe₂CH₂OH)₄]²⁻ shifts monotonically from −1.23 V in DMF to −1.09 V in methanol and to −0.83 V in aqueous solution. This effect is very likely due to hydrogen bonding of solvent to sulfur atoms of the cluster, thereby decreasing the
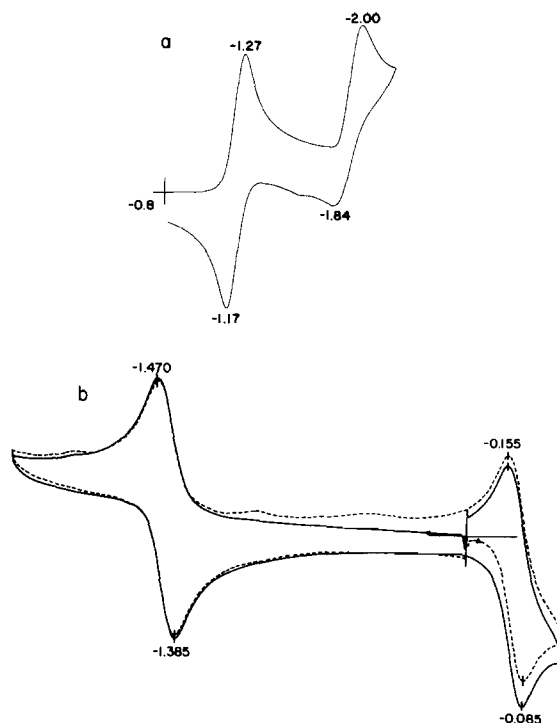
energy required to stabilize the added negative charge in the absence of hydrogen bond donors. Substituent dependence is illustrated by $E_{1/2}$ (2−/3−) = −1.42 V (R = t-Bu) and −1.23 V (R = CMe₂CH₂-OH) in DMF. For a larger number of cases the linear free energy relationship $E_{1/2}(2−/3−) = 0.298\sigma_p − 1.03$ (V) has been observed between reversible potentials in DMF and Hammett constants [46]. This merely expresses the trend that more strongly electron-donating substituents afford the more negative potentials. Indeed, $E_{1/2}(2−/3−) = −1.48$ V for [Fe₄S₄(SC₆H₁₀-1-Me)₄]²⁻ is the lowest potential yet observed for this couple.

Oxidation

Both solvent and substituent effects on the oxidation of [Fe₄S₄(SR)₄]²⁻ clusters have been examined. In DMF solution at a platinum or glassy carbon electrode all clusters exhibit multi-electron oxidation reactions at potentials more positive than ∼0 V. This result is perhaps not surprising in view of the fact that a cluster contains a reservoir of 14 electrons susceptible to removal in the processes 4RS⁻ → 2RSSR, 4S²⁻ → 4S°, and 2Fe(II) → 2Fe(III). Only with t-alkyl substituents were

discrete oxidation processes observed at less negative potentials. The DP polarogram of $[Fe_4S_4(S\text{-}t\text{-}Bu)_4]^{2-}$ shown in Fig. 3c contains a well-defined feature at -0.14 V followed by another peak at $+0.10$ V and then massive oxidation. The area of first peak, whose potential is in reasonable agreement with $E_{1/2} = -0.12$ V found earlier by dc polarography [5], has a deconvoluted area which is essentially equal to that of the $2-/3-$ reduction step at -1.43 V. On this basis the -0.14 V peak is assigned to a one-electron oxidation, presumably $2-/1-$. Discrete oxidation peaks in the same potential region were observed for two other R = t-alkyl clusters (Table I). The origin of the peak at $+0.10$ V is unknown. Addition of methanol to DMF solutions of t-alkyl clusters caused the large oxidation features above 0 V to shift to more positive potentials and diminish in intensity without much altering the initial oxidation process. This behavior is illustrated for $[Fe_4S_4(SCMe_2CH_2OH)_4]^{2-}$ in Fig. 3cd. In 1:1 v/v DMF/MeOH the area of the oxidative feature at -0.08 V is nearly equal to that of well-defined $2-/3-$ reduction at -1.16 V. Because of the greater stability of clusters in aprotic solvents further examination of cluster oxidation was restricted to DMF solutions.

When examined by CV in DMF over a potential interval one limit of which was no more positive than 0 V, $[Fe_4S_4(S\text{-}t\text{-}Bu)_4]^{2-}$ exhibited a well-defined oxidation process regardless of the initial scan direction from the potential of zero current. Voltammograms are displayed in Fig. 4b. For this oxidation $E_{1/2} = -0.12$ V and $\Delta E_p = 70$ mV, the latter being close to the value (59 mV) for reversible one-electron transfer. The electrochemical near-reversibility eliminates the possibility that the oxidation process is that of bound or dissociated thiolate to disulfide, inasmuch as such reactions are electrochemically irreversible [47]. Consequently, the CV observations support the existence of a reversible oxidation of the intact cluster.

Coulometric oxidation at a potential just positive of -0.05 V was attempted in order to substantiate further a one-electron reaction and to generate $[Fe_4S_4(S\text{-}t\text{-}Bu)_4]^{1-}$. A discrete one-electron process was not found. After passage of 3–4 electrons/cluster the oxidation was stopped, at which time the current was considerably above background level, the solution was turbid, and the odor of di-t-butyldisulfide was evident. The CV of the solution at this point did not contain the -0.12 V oxidation and the large irreversible oxidation features at more positive potentials increased in intensity. In addition, a broad irreversible reduction centered at -0.65 V, attributed to di-t-butyldisulfide by comparison with an authentic sample, appeared. Cessation of coulometric oxidation after removal of one electron/cluster followed by CV revealed diminution of the -0.12 V

oxidation step, an increase in oxidation current at more positive potentials, and the appearance of a small disulfide reduction peak. Treatment of $[Fe_4S_4(S\text{-}t\text{-}Bu)_4]^{2-}$ in DMF with the relatively weak chemical oxidants p-chloroanil ($E_{1/2} = 0.10$ V), $Ru(CF_3COCHCOPh)_3$ [48] ($E_{1/2} = 0.12$ V), and $[Fe(C_5H_5)]^+$ ($E_{1/2} = 0.40$ V) afforded results similar to those of electrochemical oxidation. Addition of one equiv. of each oxidant diminished the -0.12 V step in CV and produced some disulfide. Addition of 2–3 equiv. eliminated the -0.12 V oxidation feature, caused turbidity, and increased the amount of disulfide.

The foregoing observations lead to the conclusion that $[Fe_4S_4(S\text{-}t\text{-}Bu)_4]^{1-}$ is an authentic species subject to reversible formation and reduction at $E_{1/2} = -0.12$ V in DMF *on the CV time scale*. Although not examined in detail by CV the one-electron oxidations of two other clusters at nearly the same potential (Table I) suggest the existence of $[Fe_4S_4(SCMe_2CH_2NHPh)_4]^{1-}$ and $[Fe_4S_4(SCMe_2CH_2OH)_4]^{1-}$. Because one member ($2-$ cluster) has been isolated and the other three detected electrochemically, the electron transfer series (1) for R = t-Bu, CMe_2CH_2NHPh, and CMe_2CH_2OH may be considered complete in the sense that it spans all known core oxidation levels of biological occurrence. Clearly, oxidized clusters have very limited stability and the production of solutions with standing concentrations of $[Fe_4S_4(SR)_4]^{1-}$ appears unlikely, at least at ambient temperature. It is possible that the $[Fe_4S_4]^{3+}$ core is a sufficiently strong oxidant to produce disulfide from bound thiolate, thereby initiating a decompositon reaction of the incompletely ligated core. This may be only one of several instability factors inasmuch as $[Fe_4S_4Cl_4]^{2+}$ [49] fails to show a discrete oxidation reaction by DPP or CV. As recognized by others [13], the paramagnetic species produced by fast oxidation and freezing of aqueous solutions initially containing $[Fe_4S_4]^{2-}$ clusters [13, 50] may not be $[Fe_4S_4(SR)_4]^{1-}$. Based on the observations here of very limited stability of oxidized clusters and the inability, thus far, to accomplish reversible one-electron oxidations of protein $[Fe_4S_4]^{2+}$ sites except in the HP case, it is quite evident that proteins of the latter type provide special structural and environmental factors. These not only permit reversible oxidation reactions but afford appreciable temporal stability of HP_{ox} ($[Fe_4S_4]^{3+}$) sites. At the same time these factors do not allow reduction to the $HP_{s\text{-}red}$ form (series (1)) except under conditions of protein unfolding [51]. Achievement of stable analogues of HP_{ox} sites is likely to be a formidable task and may require polydentate thiolate ligands that promote the stability of the oxidized core. Tetracysteinyl cyclic peptides [52] represent one interesting possibility. Lastly, the observation of $2-/1-$ cluster

oxidations with R = t-alkyl is almost certainly a consequence of the electron-releasing property of these substituents. As already noted, this property causes cathodic displacements of 2−/3− potentials. It apparently has the same effect on 1−/2− potentials, shifting them to values just negative of the potentials at which multi-electron oxidations occur. Certainly there is no structural feature of $[Fe_4S_4(S\text{-}t\text{-}Bu)_4]^{2-}$ (in the solid state) compared to other clusters that is especially conducive to oxidation.

Acknowledgements

References

1 R. H. Holm and J. A. Ibers, in W. Lovenberg, (Ed.), 'Iron−Sulfur Proteins', Academic Press, New York, 1977, chap. 7.

2 R. H. Holm, Acc. Chem. Res., 10, 427 (1977).

3 J. A. Ibers and R. H. Holm, Science, 209, 223 (1980).

4 J. M. Berg and R. H. Holm, in T. G. Spiro, (Ed.), 'Metal Ions in Biology', Vol. 4, 'Iron−Sulfur Proteins', Wiley−Interscience, New York, 1982, chap 1.

5 B. V. DePamphilis, B. A. Averill, T. Herskovitz, L. Que, Jr., and R. H. Holm, J. Am. Chem. Soc., 96, 4159 (1974).

6 J. Cambray, R. W. Lane, A. G. Wedd, R. W. Johnson and R. H. Holm, Inorg. Chem., 16, 2565 (1977).

7 B. A. Averill, T. Herskovitz, R. H. Holm and J. A. Ibers, J. Am. Chem. Soc., 95, 3523 (1973).

8 G. Christou and C. D. Garner, J. Chem. Soc., Dalton Trans., 1093 (1979).

9 K. S. Hagen, J. G. Reynolds and R. H. Holm, J. Am. Chem. Soc., 103, 4054 (1981).

10 L. Que, Jr., M. A. Bobrik, J. A. Ibers and R. H. Holm, J. Am. Chem. Soc., 96, 4168 (1974).

11 H. L. Carrell, J. P. Glusker, R. Job and T. C. Bruice, J. Am. Chem. Soc., 99, 3683 (1977).

12 M. A. Bobrik, K. O. Hodgson and R. H. Holm, Inorg. Chem., 16, 1851 (1977).

13 G. Christou, C. D. Garner, M. G. B. Drew and R. Cammack, J. Chem. Soc., Dalton Trans., 1550 (1981).

14 M. A. Bobrik, E. J. Laskowski, R. W. Johnson, W. O. Gillum, J. M. Berg, K. O. Hodgson and R. H. Holm, Inorg. Chem., 17, 1402 (1978).

15 E. J. Laskowski, R. B. Frankel, W. O. Gillum, G. C. Papaefthymiou, J. Renaud, J. A. Ibers and R. H. Holm, J. Am. Chem. Soc., 100, 5322 (1978).

16 J. M. Berg, K. O. Hodgson and R. H. Holm, J. Am. Chem. Soc., 101, 4586 (1979).

17 D. W. Stephan, G. C. Papaefthymiou, R. B. Frankel and R. H. Holm, Inorg. Chem., 22, 1550 (1983).

18 C. D. Stout, in T. G. Spiro, (Ed.), 'Metal Ions in Biology', Vol. 4, 'Iron−Sulfur Proteins', Wiley−Interscience, New York, 1982, Chap. 3.

19 L. L. Nelson, F. Y.-K. Lo, A. D. Rae and L. F. Dahl, J. Organometal. Chem., 225, 309 (1982).

20 W. V. Sweeney, A. J. Bearden and J. C. Rabinowitz, Biochem. Biophys. Res. Commun., 59, 188 (1974).

21 W. V. Sweeney, J. C. Rabinowitz and D. C. Yoch, J. Biol. Chem., 250, 7842 (1975).

22 A. J. Thomson, A. E. Robinson, M. K. Johnson, R. Cammack, K. K. Rao and D. O. Hall, Biochim. Biophys. Acta, 637, 423 (1981).

23 M. K. Johnson, T. G. Spiro and L. E. Mortenson, J. Biol. Chem., 257, 2447 (1982).

24 M. H. Emptage, T. A. Kent, B.-H. Huynh, J. Rawlings, W. H. Orme-Johnson and E. Münck, J. Biol. Chem., 255, 1793 (1980).

25 D. Ghosh, S. O'Donnell, W. Furey, Jr., A. H. Robbins and C. D. Stout, J. Mol. Biol., 158, 73 (1982).

26 C. W. Carter, Jr., J. Kraut, S. T. Freer, N. Xuong, R. A. Alden and R. G. Bartsch, J. Biol. Chem., 249, 4212 (1974);
S. T. Freer, R. A. Alden, C. W. Carter, Jr., and J. Kraut, ibid., 250, 46 (1975).

27 K. W. Merz and M. Speckar, Arch. Pharm., 296, 427 (1963).

28 R. W. Johnson and R. H. Holm, J. Am. Chem. Soc., 100, 5338 (1978).

29 C. G. Moore and R. W. Saville, J. Chem. Soc., 2089 (1954).

30 E. Baumann and E. Fromm, Chem. Ber., 28, 910 (1895).

31 R. H. Holm, W. D. Phillips, B. A. Averill, J. J. Mayerle and T. Herskovitz, J. Am. Chem. Soc., 96, 2109 (1974).

32 C. L. Hill, J. Renaud, R. H. Holm and L. E. Mortenson, J. Am. Chem. Soc., 99, 2549 (1977).

33 M. Rzaigui, R. Panossian and D. Benlian, Rev. Chim. Mineral., 17, 586 (1980).

34 R. C. Job and T. C. Bruice, Proc. Natl. Acad. Sci. U.S.A., 72, 2478 (1975).

35 R. Maskiewicz and T. C. Bruice, J. Chem. Soc., Chem Commun., 703 (1978).

36 M. W. W. Adams, S. G. Reeves, D. O. Hall, G. Christou, B. Ridge and H. N. Rydon, Biochem. Biophys. Res. Commun., 79, 1184 (1978).

37 W. E. Cleland and B. A. Averill, Inorg. Chim. Acta, 56, L9 (1981).

38 W. E. Cleland, D. A. Holtman, M. Sabat, J. A. Ibers and B. A. Averill, J. Am. Chem. Soc., submitted for publication.

39 J. M. Berg, results to be published.

40 C. H. Wei, G. R. Wilkes, P. M. Treichel and L. F. Dahl, Inorg. Chem., 5, 900 (1966);
R. A. Shunn, C. J. Fritchie, Jr., and C. T. Prewitt, ibid., 5, 892 (1966).

41 Trinh-Toan, B.K. Teo, J. A. Ferguson, T. J. Meyer and L. F. Dahl, J. Am. Chem. Soc., 99, 408 (1977).

42 A. Aizman and D. A. Case, J. Am. Chem. Soc., 104, 3269 (1982).

43 C. Y. Yang, K. H. Johnson, R. H. Holm and J. G. Norman, Jr., J. Am. Chem. Soc., 97, 6596 (1975).

44 R. E. Johnson and R. H. Holm, results to be published.

45 E. J. Laskowski, J. G. Reynolds, R. B. Frankel, S. Foner, G. C. Papaefthymiou and R. H. Holm, J. Am. Chem. Soc., 101, 6562 (1979).

46 J. J. Mayerle, S. E. Denmark, B. V. DePamphilis, J. A. Ibers and R. H. Holm, J. Am. Chem. Soc., 97, 1032 (1975).

47 J. R. Bradbury, A. F. Masters, A. C. McDonell, A. A. Brunette, A. M. Bond and A. G. Wedd, J. Am. Chem

Soc., 103, 1959 (1981), and references therein.

48 G. S. Patterson and R. H. Holm, *Inorg. Chem., 11*, 2285 (1972).

49 G. B. Wong, M. A. Bobrik and R. H. Holm, *Inorg. Chem., 17*, 587 (1978).

50 R. Cammack and G. Christou, in H. H. Schlegel and K. Schneider, (Ed.), 'Hydrogenases: Their Catalytic Activity, Structure and Function', E. Göltze Verlag, Göt-

tingen, 1978, pp. 45–56.

51 R. Cammack, *Biochem. Biophys. Res. Commun., 54*, 548 (1973). The HP_{red}/HP_{s-red} reduction in aqueous solution by pulse radiolysis has been described: J. Butler, A. G. Sykes, G. V. Buxton, P. C. Harrington and R. G. Wilkins, *Biochem. J., 189*, 641 (1980).

52 N. Ohta, C. Kawasaki, M. Maeda, S. Tani and K. Kawasaki, *Chem. Pharm. Bull., 27*, 2968 (1979).